Modular Graphene-Based 3D Covalent Networks: Functional Architectures for Energy Applications

Xiaoyan Zhang, Artur Ciesielski, Fanny Richard, Pengkun Chen, Eko Adi Prasetyanto, Luisa de Cola, Paolo Samorì

DOI: 10.1002/ ((please add manuscript number))
Article type: (Full Paper)

Modular Graphene-based 3D Covalent Networks: Functional Architectures for Energy Applications

*Xiaoyan Zhang, Artur Ciesielski, Fanny Richard, Pengkun Chen, Eko Adi Prasetyanto, Luisa De Cola and Paolo Samorì**

ISIS & icFRC, Université de Strasbourg & CNRS, 8 allée Gaspard Monge, 67000 Strasbourg, France.

Keywords: graphene, network, supercapacitor, energy applications

The development of ordered graphene-based materials combining high stability, large surface areas, ability to act as absorbent of relevant chemical species and solution processability is of significance for energy applications. A poorly explored approach relies on the controlled nanostructuration of graphene into robust and highly ordered three-dimensional (3D) networks as a route to further leverage the exceptional properties of this unique material. Here, we report a simple yet effective and scalable one-step method to prepare graphene-based 3D covalent networks (G3DCNs) with tunable interlayer distance *via* controlled polymerization of benzidines with graphene oxide (GO) at different reactions temperatures under catalyst- and template-free conditions. The reduced form of G3DCNs (RG3DCNs) was used as electrodes in supercapacitors; it revealed a high specific capacitance of 156 F g^{-1} at a current density of 1 A g^{-1} in a two-electrode configuration and 460 F g^{-1} at a current density of 0.5 A g^{-1} in a three-electrode configuration, combined with an excellent cycling stability over 5000 cycles. The present study will promote the quantitative understanding of structure-properties relationship, for the controlled fabrication of 3D graphene-based multifunctional materials.

1. Introduction

Graphene,[1] a monolayer of graphite arranged in a hexagonal lattice, has attracted a notable attention over the past few years due to its outstanding optical, mechanical, thermal and electrical properties which makes it a promising material for various applications ranging from electronic devices, to composites and energy related applications.[2-9] Graphene and its derivatives are being considered ideal candidates for energy related applications because of their large accessible specific surface areas and high electrical conductivity.[2] The theoretical value of the specific surface area of graphene is close to 2600 m^2 g^{-1}.[10] However, a common problem encountered is the re-stacking, *i.e.*, the aggregation of the graphene sheets during the wet-processing, yielding in a drastic decrease of the effective specific surface area, and consequently of the performance of the materials.[11] For example, the reduction of graphene oxide (GO) without surface modification normally leads to the irreversible aggregation of the graphene sheets.[12] In order to solve this problem, the bridging of two-dimensional (2D) graphene layers into three-dimensional (3D) macroscopic porous structures is an essential step in order to tailor graphene-based multifunctional materials, which could preserve many of the unique properties of the individual graphene sheets.[13] Theoretical and experimental results showed that 3D graphene-based functional materials possess high specific surface areas and porous structures. These features are key components for a wide range of applications, such as catalysis, gas adsorption and energy storage,[14,15] and also holds potential for exploring and tuning fundamental physical and chemical properties of molecular materials in confined space. For instance, the high specific surface area and porous structures can provide a large amount of space for hosting electrolyte ions, therefore increasing the capacitance performance in supercapacitors.[16] In this context, the fabrication of 3D graphene-based networks through covalent linkage between individual graphene sheets is one amongst the greatest challenges in the field, resulting in a high control over the structures with a nanoscale precision and consequently tuning of the material's physical properties.[17-20] Although 3D graphene-based

covalent networks have been previously prepared by changing the length of the starting diamines reacting with GO,[21,22] hitherto there are no reports on the generation of tunable covalent networks made by combining GO with a *single* reagent, by exploiting the ability of the latter component to undergo oligomerization when exposed to different experimental conditions.

Hitherto, graphene can be produced in several ways, including mechanical cleavage,[1] epitaxial growth,[23-26] solvent-assisted exfoliation of graphite[27-33] and reduction of GO.[34-36] Among them, chemical oxidation and exfoliation of graphite into GO is still the most popular method. GO is the highly oxidized form of graphene obtained by treating graphite with strong oxidizers, the latter also promoting intercalation and exfoliation. GO exposes variety of oxygen functional groups such as carbonyl, epoxy and hydroxyl, which make it an ideal candidate for building graphene-based macroscopic porous structures through simple chemical reactions.[37]

In this paper, we describe a simple and efficient method for the facile preparation of graphene-based 3D covalent networks with adjustable interlayer distance upon covalent functionalization of GO. This method relies on the condensation and ring-opening reactions, at different temperatures, of the carbonyl and epoxy groups on GO with benzidine. Noteworthy, for the first time, the controlled polymerization of benzidines with GO, to obtain the graphene-based 3D covalent networks (G3DCNs), was performed under catalyst- and template-free conditions. By varying the reaction temperatures, benzidine monomers or polymerized benzidine (PBZ) units can bridge GO sheets to form 3D covalent networks with tunable interlayer spacing. The use of the reduced form of the G3DCNs (RG3DCNs) was used to develop high performance supercapacitors, taking advantage of the high specific surface areas combined with the nitrogen doping obtained through the chemical functionalization.

2. Results and Discussions

Benzidine contains two $–NH_2$ groups that can react with carbonyl and in particular with epoxy groups on GO *via* nucleophilic additions. Furthermore, it is also reported that GO itself can act as a catalyst to promote organic reactions by taking advantage of GO's acidity and/or oxidation potential.[38,39] Therefore, GO's acidity is also expected to promote the nucleophilic reaction of benzidine in the present case. The G3DCNs were synthesized by reacting the same concentrations of GO with benzidine in ethanol/water mixture (1:1) at different temperatures, *i.e.* room temperature (G3DCN-**1**), 45 °C (G3DCN-**2**) and 80 °C (G3DCN-**3**). Given that in our experiment we used an excess of benzidine and that the diffusion of benzidine is much faster than that of GO, all GOs are expected to react. In order to purify these samples, *i.e.* to remove benzidine monomers and/or polymerized benzidines not reacted with GO, the samples were extensively washed with a copious amount of *N,N*-dimethylformamide (DMF) and ethanol until the supernatant is colorless. The scheme of the reaction as well of the chemical structures of the three obtained G3DCNs are shown in Figure 1.

All the structures obtained have been investigated using different spectroscopies. Figure 2a portrays the UV/Vis absorption spectra of benzidine, G3DCN-**1**, G3DCN-**2**, G3DCN-**3** and neat GO. The latter shows a shoulder peak at λ = 305 nm, which is attributed to the n-π^* transition of the C=O moiety.[40] Benzidine displays an absorption peak at λ = 285 nm, while G3DCN-**1** shows a broad peak at λ = 300 nm which can be assigned to the overlying spectral features of benzidine units chemically tethered to GO and the C=O groups of GO. Conversely, G3DCN-**2** and G3DCN-**3** exhibit an absorption peak at λ = 296 and λ = 303 nm, respectively. More importantly, both of them show a broad absorption band within the range of 600 and 700 nm. These broad bands are ascribed to the characteristic absorption of the PBZ-based oligomers.[41] Also, G3DCN-**3**'s spectra is more red-shifted compared with that of G3DCN-**2**, indicating that the degree of polymerization of benzidine in G3DCN-**3** is higher if compared

to G3DCN-**2**, as a result of the enhanced degree of polymerization of benzidines at high temperatures. The latter is reflected in change in the 3D structure, in particular in the interlayer distance within the graphene-based 3D covalent networks. Such changes in the interlayer distance (d_{002}) were characterized by wide-angle X-ray scattering (WAXS), as shown in Figure 2b. The starting material of GO displays a typical sharp peak at ~ 11.6°, corresponding to an interlayer spacing of 0.76 nm due to the (002) reflection of stacked GO sheets, in accordance with the values reported previously.[42-44] The 2θ peak of the as-prepared 3D functionalized graphene-based networks shifts towards lower angles (10.1°, 8.6° and 6.9° for G3DCN-**1**, G3DCN-**2** and G3DCN-**3**, respectively) indicating an increasingly higher interlayer distance compared to GO. Based on the Bragg equation, the d_{002} spacing was calculated being 0.87, 1.02 and 1.27 nm for G3DCN-**1**, G3DCN-**2** and G3DCN-**3**, respectively. This indicates the successful anchoring of benzidine/PBZ units between the GO sheets. While the theoretical length of benzidine is calculated to be ~ 0.94 nm, in the case of G3DCN-**1**, the interlayer distance is 0.11 nm greater than in GO. This means that the benzidines pillars are not arranged perpendicular to the GO layers, but are bound randomly with certain tilt angles towards GO layers. The situation is similar for G3DCN-**2** and G3DCN-**3**. This is reasonable because the benzidine/PBZ units have to find the partner reacting groups on two different GO sheets in order to link them covalently, in a reaction occurring under kinetic control.

Figure 2c shows the FTIR spectra of GO, G3DCN-**1**, G3DCN-**2** and G3DCN-**3**. The spectrum of GO displays its well-known features, *i.e.*, C=O stretching at 1731 cm^{-1}, C=C stretching at 1620 cm^{-1}, C-O-H bending at 1409 cm^{-1}, C-O stretching at 1223 cm^{-1} and C-O-C stretching of epoxy groups at 1047 cm^{-1}. After reaction, the epoxy groups in the GO disappear, and a new band at 1034, 1018, 1018 cm^{-1} appears in G3DCN-**1**, G3DCN-**2** and G3DCN-**3**, respectively. This band is attributed to the C-N stretching mode. Also, the relative intensity of the C=O groups present in the starting materials of GO notably decreases, probably because of the

occurrence of a condensation reaction between the C=O and NH_2 groups to form imines. The disappearance of epoxy and reduction of the carbonyl groups confirm the successful covalent linkage between GO and the reagents. It should be also pointed that the content of the remaining oxygen groups decreased gradually from G3DCN-**1**, G3DCN-**2** to G3DCN-**3**, indicating that the degree of reduction of GO during the reaction increases with the temperature.

The thermal stability behavior of GO, G3DCN-**1**, G3DCN-**2** and G3DCN-**3** was investigated by thermal gravimetric analysis (TGA) running under nitrogen atmosphere, as portrayed in Figure 1d. GO displays a weight loss ~ 30% between 200 and 300 °C, which is due to the decomposition of the oxygen functional groups such as carboxyl, carbonyl, hydroxyl and epoxy of GO.[45] Further mass loss of ~ 35% occurs heating the sample up to 900 °C, leading to an overall residual mass of 35%. Compared with GO, the three G3DCNs show an increase of thermal stability, with G3DCNs-**3** being the most stable one. The residual mass at 900 °C amounts to 52%, 60% and 74% for G3DCN-**1**, G3DCN-**2** and G3DCN-**3**, respectively. The improved thermal stability can be attributed to the reduction of GO which increases with the reaction temperature during the G3DCN formation.

X-ray Photoelectron Spectroscopy (XPS) provided a compositional characterization by identifying the relevant chemical elements present in both GO and G3DCNs. Figure 3 portrays the N1s XPS spectra of GO, G3DCN-**1**, G3DCN-**2** and G3DCN-**3**. The N1s spectrum of GO displays only noise, indicating negligible nitrogen content. In contrast, the intensity of the N1s signal of the three G3DCNs provides evidence for an obvious increase in nitrogen content, amounting to about 3.1%, 3.8%, 6.4% for G3DCN-**1**, G3DCN-**2** and G3DCN-**3**, respectively (see Supplementary Table S1). For all the three G3DCNs, the N1s spectra can be deconvoluted to two peaks: the one at ~ 399 eV can be attributed to -NH, and the peak around 401 eV can be assigned to imine groups.[46,47] The content of –NH increases gradually from G3DCN-**1**, G3DCN-**2** to G3DCN-**3**, highlighting the formation of PBZ acting

as bridges between the GO sheets. Furthermore, the C/O ratio also increases from GO, G3DCN-**1**, G3DCN-**2** to G3DCN-**3** (see Supplementary Table S1). Based on the results from Table S1, for G3DCN-**1** (not polymerized) every 30.1 carbon atoms have one benzidine (see supporting information for the details on the calculations). Conversely, for G3DCN-2 and G3DCN-3, it is very difficult to determine the polymerization degree of the PBZ in the G3DCN, therefore for these two cases the functionalization degree has not been quantified.

As a further characterization we have employed Raman spectroscopy, which is a powerful tool to characterize graphitic materials, and compared the spectra of GO with the three G3DCNs materials. For GO, the characteristic Raman bands are: a disorder-induced D band at ~ 1350 cm^{-1} and an in-plane vibration mode of sp^2 hybridized carbon at ~ 1580 cm^{-1} (see Supplementary Figure S4). For the three G3DCNs, all the Raman spectra still keep the feature of GO, showing both D and G bands. It is worth mentioning that additional bands are observed in the Raman spectra of the three G3DCNs (see Supplementary Figure S4, the positions are marked by asterisks). These bands are attributed to the Raman features of the bound benzidine/PBZ units.[48,49] The increase of the intensity ratio between D and G bands (I_D/I_G) is normally observed after the reduction of GO.[50] In the present case, during the reaction, GO was also reduced to some extent as revealed by FTIR and TGA. However, for the three G3DCNs samples, the I_D/I_G ratio is almost unchanged or even shows a decrease compared to GO. This can be explained by the contribution from the benzidine/PBZ units,[48,49] whose bands are overlapping with the G band of GO.

To get a morphological insight into our different materials, scanning electron microscopy (SEM) images were recorded for G3DCN-**1**, G3DCN-**2** and G3DCN-**3**. Figure 4 clearly shows that all three samples, *i.e.* (a,b) G3DCN-**1**, (c, d) G3DCN-**2**, (e,f) G3DCN-**3** possess highly porous surfaces. To bestow information onto the porosity, N_2 adsorption-desorption isotherms have been performed (see below). All materials have also been investigated by transmission electron microscopy (TEM) imaging. Supplementary Figure S5a shows that GO

sample is highly transparent providing evidence for the successful exfoliation in water, as also proved by atomic force microscopy (AFM) measurement (Figure S2). In contrast, the TEM images of G3DCN-**1**, G3DCN-**2** and G3DCN-**3** (see Supplementary Figure S5b, S5c and S5d) reveal the stacking of the G3DCNs sheets indicating the anchoring of the GO sheets through the benzidine pillars or PBZ units.

The porous properties of GO, G3DCN-**1**, G3DCN-**2** and G3DCN-**3** were further characterized by N_2 adsorption-desorption isotherms measurement at 77 K; the results are summarized in supplementary Table S2. The starting material of GO displays a specific surface area of ~ 199 $m^2 g^{-1}$. The specific surface area of G3DCN-**1** and G3DCN-**2** was found to be 238 and 276 $m^2 g^{-1}$, respectively. Compared with GO, the increase of the specific surface area of the G3DCN-**1** and G3DCN-**2** indicates that the interlayer cross-linkers derived from benzidine or PBZ units, acting as pillars, hinder the stacking between adjacent GO layers, leading to more accessible surface area for the adsorption of N_2 molecules. Surprisingly, the sample of G3DCN-**3** with the largest interlayer distance among the three samples does not possesses the highest specific surface area (254 $m^2 g^{-1}$). This might be due to the fact that the PBZ units are not linearly oriented and the bending of the units lead to an occupancy of the interlayer spaces between GO layers (an indication of the filled interlayer voids). The sample of G3DCN-**2** shows the largest surface area among the three G3DCNs, which can be explained by the mild degree of bridging GO layers by the PBZ units compared with G3DCN-**3**, thus preventing the restacking of GO and leaving more space between the layers. The above analysis corroborate that the density of the anchoring units is strongly affected by the reaction temperature which plays an extremely important role in determ ining the specific surface area and pore volume of the three G3DCNs.

In order to further exploit the increased specific surface area in our G3DCNs, we have carried out supercapacitor measurements using the reduced form of G3DCNs (RG3DCNs) as electrodes. The electrochemical performance was studied in 1.0 M H_2SO_4 electrolyte using a

two-electrode configuration.[51-54] The cyclic voltammetry (CV) was performed in the potential range of -0.2-0.8 V at different scan rates (see Supplementary Figure S6). All the CV curves of the three RG3DCNs show a rectangular shape, indicating an ideal capacitive behavior.[51,52] Figure 5a shows the galvanostatic charge/discharge curves of RG3DCNs at a current density of 1 A g^{-1}. The specific capacitance was calculated to be 100, 127 and 156 F g^{-1} for RG3DCN–**1**, **2** and **3**, respectively. The power density of the three RG3DCNs is calculated to be 5.27, 2.41 and 1.87 kW kg^{-1}, respectively. The volumetric capacitance of the three RG3DCNs is calculated to be 59.6, 65.1 and 68.1 F cm^{-3}, respectively. At a higher current density of 2 A g^{-1}, the value can be maintained as high as 83, 109 and 131 F g^{-1}, respectively. These values are comparable with carbon-based supercapacitors produced by activation of graphene by Ruoff and coworkers,[53] and higher than cross-linked reduced graphene oxide foam,[54] using the same two-electrode configuration. *Three-electrode configuration* was also tested for RG3DCNs at a current density of 0.5 A g^{-1}. The specific capacitance was calculated to be 369, 400 and 460 F g^{-1} for RG3DCN–**1**, **2** and **3**, respectively. These values are also higher than the previously reported on graphene/polyaniline[55,56] (301 F g^{-1} and 250 F g^{-1} at a current density of 0.5 A g^{-1}) and graphene/polyrrole[57] (285 F g^{-1} at a current density of 0.5 A g^{-1}) nanocomposites using the same three-electrode configuration. It is worth mentioning that three-electrode configurations exhibit much greater values of specific capacitance when compared to two-electrode configurations.[58] Therefore, to properly compare the results with values in literature, supercapacitors integrating a new material should be measured both in two- and three-electrode configurations. Obviously, RG3DCN-**3**, featuring the largest interlayer distance, shows the highest capacitance among the three samples. It is known that the final performance of supercapacitors is affected by several factors: the specific surface area, electrical conductivity, doping of the active materials and in particular electrode configuration, *etc*.[59] Although the electrical conductivity of RG3DCN–**3** are the lowest among the three samples,[60] the nitrogen content and specific surface area are the highest (see

Supplementary Table S3, S4 and S5).[61] In the present case, the specific surface area and nitrogen doping are considered being the key factors determining the capacitance performance of the three RG3DCNs. It is indeed known that nitrogen doping in the graphene-based electrodes contribute to the increase of the surface Faradaic reaction.[62–64] Also, it changes the electron distribution of the electrode materials, leading to a potential further improve the wettability between the electrode materials and the electrolytes, thus increasing the active surface area accessible to the electrolyte.[65]

Electrochemical impedance spectroscopy (EIS) was also performed, as presented in Figure 5b. At high frequency (close to 100 kHz, Figure 5c), the intersection point on the X-axis stands for the Ohmic resistance of the electrolyte and the internal resistance of the electrode, defining as R_S. The value of R_S is 0.48, 0.49, and 0.52 Ω for RG3DCN–**1**, **2** and **3**, respectively, suggesting a low ohmic resistance of the electrolyte and the internal resistance of the electrode, which is an important parameter affecting the performance of supercapacitors.[66] The cycle stability is also of paramount importance for practical applications of supercapacitors, and was evaluated through charge-discharge cycles at a current density of 1 A g^{-1}. Remarkably, no obvious specific capacitance loss was recorded for all the three RG3DCNs working electrodes after 5000 cycles (Figure 5d), demonstrating their high stability, long cycle lifetime and good reversibility as working electrodes in supercapacitors.

The high specific capacitance of RG3DCNs is attributed to the synergistic effect of the high specific surface area (due to the formation of 3D porous covalent networks), good electrical conductivity and introduction of nitrogen doping. The presence of macro- and mesopores 3D structures can favor the ion transport and charge storage at the interface between the electrodes and electrolyte ions. The macropores can play a role as a buffering reservoir for the fast diffusion of electrolyte to inner surface of the pores, and the mesopores can facilitate the

ion transport and charge storage *via* providing a large accessible surface area.[67] The anchored benzidine or PBZ units may also contribute to the charge transfer process between the electrodes and the electrolyte ions.

3. Conclusions

In summary, graphene-based 3D covalent networks with tunable interlayer distance can be prepared *via* controlled polymerization of benzidines with graphene oxide at different reaction temperatures under catalyst- and template-free conditions. The as-prepared three G3DCNs samples show tunable specific surface area and porosity. The specific capacitances determined using reduced form of G3DCNs (RG3DCNs) as electrodes in supercapacitors are very promising. While in three-electrode configuration it resulted 460 F g^{-1} at a current density of 0.5 A g^{-1}, in two-electrode configuration it amounted to 156 F g^{-1} at a current density of 1 A g^{-1} in combination with an excellent cycling stability over 5000 cycles. The observed combination of excellent physicochemical stability and high supercapacitor performance, clearly demonstrate that integration of 2D graphene sheets into 3D graphene-based covalent nanostructures with tunable structures and properties is an ideal route to obtain multifunctional nanomaterials. It is anticipated that the present study will promote the quantitative understanding of structure-properties relationship, for the controlled fabrication of 3D graphene-based multifunctional materials, and will further pave a promising way for potential applications towards clean energy storage.[68]

4. Experimental Section

Characterization: UV/Vis spectra were recorded using a JASCO V-670 UV/Vis Spectrometer. Fourier Transform Infrared Spectroscopy (FTIR) were collected using a Thermo Scientific Nicolet 6700 FTIR Spectrometer equipped with a Smart Orbit accessory. Transmission electron microscopy (TEM) characterization was performed using a Philips CM120 operating at 120 KV. Scanning electron microscopy (SEM) was carried out using an FEI Quanta 250

FEG instrument. Atomic force microscopy (AFM) was performed on a Veeco Dimension 3100 operating on a Nanoscope IV control unit. Raman spectra were recorded on a custom-made setup Spectrometer (excitation at 532 nm). Thermal gravimetric analysis (TGA) was performed under N_2 atmosphere on a Mettler Toledo TGA/SDTA851e system. The specific surface area was measured using a Micromeritics ASAP 2050 surface area and porosity analyzer. Nitrogen adsorption and desorption isotherm was measured at 77 K. Wide-angle X-ray scattering (WAXS) was performed on a SAXSess X-Ray Scattering instrument (Anton Paar GmbH, Austria). A Thermo Scientific K-Alpha X-ray Photoelectron Spectrometer (XPS) using monochromatic AlKα radiation (hν = 1486.6 eV) was used to investigate the surface properties. High-resolution measurements were performed with a 50 eV analyser pass energy and a 0.1 eV energy step size to get N1s spectra. Electrical conductivity was conducted on a JANDEL (Model RM3000) instrument using the four-point probe method. Film thickness was determined by Alpha-Step IQ surface profiler (LOT ORIEL Group).

Materials: Graphene oxide (GO, Graphenea), benzidine (97%, Sigma-Aldrich), hydrazine monohydrate (30% in water, Sigma-Aldrich), polyvinylidene difluoride (Sigma-Aldrich) and carbon black (Sigma-Aldrich) were used as received without further purification.

Preparation of G3DCNs and RG3DCNs: In a typical experiment, GO (80 mg) in water (50 ml) and benzidine (500 mg) in ethanol (50 ml) were mixed together, and the reaction mixture was reacted at room temperature/45 ºC/80 ºC for 24 h. After the reaction, the reaction mixture was centrifuged and washed with copious amount of organic solvents (DMF and ethanol) until the supernatant is colorless, confirming the absence of unreacted reagents. Finally, the solids were dried in vacuum to obtain the desired products, named as G3DCN-**1**, G3DCN-**2** and G3DCN-**3**.

For the chemical reduction of G3DCN-**1**, G3DCN-**2** and G3DCN-**3**, the three samples were treated with hydrazine monohydrate (30% in water) at 80 ºC for 24 h.[69] The obtained

RG3DCN-**1**, RG3DCN-**2** and RG3DCN-**3** were dried in vacuum and directly used as active materials for the supercapacitor measurements.

Electrochemical measurements: Electrochemical measurements were performed on a PGSTAT204 instrument (Autolab). The electrochemical measurements were conducted in 1.0 M H_2SO_4 electrolyte using both a two-electrode and a three-electrode (platinum as the counter electrode and Ag/AgCl as the reference electrode) configuration. The electrodes were prepared by mixing RG3DCNs with carbon black and polyvinylidene difluoride (PVDF). High mass loading (~ 10 mg) was used to fabricate the electrodes according to the method described by Ruoff and coworkers,[70] as also discussed by Gogotsi and Simon.[71]

Supporting Information
Supporting Information is available from the Wiley Online Library or from the author.

Acknowledgements
This work was supported by the European Commission through the Graphene Flagship (GA-604391), the FP7-NMP-2012-SMALL-6 "SACS" project (GA-310651), the ERC Advanced Grant MaGIC (GA-247365), the Agence Nationale de la Recherche through the LabEx CSC (ANR-10-LABX-0026_CSC), the International Center for Frontier Research in Chemistry (icFRC). Dr. Stéphane Berciaud and Dr. Marco Gobbi are thanked for the assitance with the Raman measurement. Dr. Cécilia Menard-Moyon and Dr. Alberto Bianco are acknowledged for the preliminary study on TGA measurement.

Received: ((will be filled in by the editorial staff))
Revised: ((will be filled in by the editorial staff))
Published online: ((will be filled in by the editorial staff))

[1] K. S. Novoselov, A. K. Geim, S. V. Morozov, D. Jiang, Y. Zhang, S. V. Dubonos, I. V. Grigorieva, A. A. Firsov, *Science* **2004**, *306*, 666.

[2] F. Bonaccorso, L. Colombo, G. Yu, M. Stoller, V. Tozzini, A. C. Ferrari, R. S. Ruoff, V. Pellegrini, *Science* **2015**, *347*, 1246501.

[3] C. N. R. Rao, A. K. Sood, K. S. Subrahmanyam, A. Govindaraj, *Angew. Chem. Int. Ed.* **2009**, *48*, 7752.

[4] a) C. Z. Yuan, L. Yang, L. R. Hou, J. Y. Li, Y. X. Sun, X. G. Zhang, L. F. Shen, X. J. Lu, S. L. Xiong, X. W. Lou, *Adv. Funct. Mater.* **2012**, *22*, 2560; b) X. Zang, Q. Chen, P. Li, Y. He, X. Li, M. Zhu, X. Li, K. Wang, M. Zhong, D. Wu, H. Zhu, *Small* **2014**, *10*, 2583; c) L. Wei, M. Sevilla, A. B. Fuertes, R. Mokaya, G. Yushin, *Adv. Funct. Mater.* **2012**, *22*, 827.

[5] P. Simon, Y. Gogotsi, *Acc. Chem. Res.* **2013**, *46*, 1094.

[6] a) G. Eda, M. Chhowalla, *Adv. Mater*. **2010**, *22*, 2392; b) Y. Huang, J. Liang, Y. Chen, *Small* **2012**, *8*, 1805; c) W. Jiang, D. Yu, Q. Zhang, K. Goh, L. Wei, Y. Yong, R. Jiang, J. Wei, Y. Chen, *Adv. Funct. Mater.* **2015**, *25*, 1063.

[7] A. C. Ferrari, F. Bonaccorso, V. Fal'ko, K. S. Novoselov, S. Roche, P. Boggild, S. Borini, F. H. L. Koppens, V. Palermo, N. Pugno, J. A. Garrido, R. Sordan, A. Bianco, L. Ballerini, M. Prato, E. Lidorikis, J. Kivioja, C. Marinelli, T. Ryhanen, A. Morpurgo, J. N. Coleman, V. Nicolosi, L. Colombo, A. Fert, M. Garcia-Hernandez, A. Bachtold, G. F. Schneider, F. Guinea, C. Dekker, M. Barbone, Z. Sun, C. Galiotis, A. N. Grigorenko, G. Konstantatos, A. Kis, M. Katsnelson, L. Vandersypen, A. Loiseau, V. Morandi, D. Neumaier, E. Treossi, V. Pellegrini, M. Polini, A. Tredicucci, G. M. Williams, B. H. Hong, J.-H. Ahn, J. M. Kim, H. Zirath, B. J. van Wees, H. van der Zant, L. Occhipinti, A. Di Matteo, I. A. Kinloch, T. Seyller, E. Quesnel, X. Feng, K. Teo, N. Rupesinghe, P. Hakonen, S. R. T. Neil, Q. Tannock, T. Lofwander, J. Kinaret, *Nanoscale* **2015**, *7*, 4598.

[8] a) M. H. Yu, Y. C. Huang, C. Li, Y. X. Zeng, W. Wang, Y. Li, P. P. Fang, X. H. Lu, Y. X. Tong, *Adv. Funct. Mater.* **2015**, *25*, 324; b) W. B. Wan, L. L. Li, Z. B. Zhao, H. Hu, X. J. Hao, D. A. Winkler, L. C. Xi, T. C. Hughes, J. S. Qiu, *Adv. Funct. Mater.* **2014**, *24*, 4915; c) X. Ou, L. Jiang, P. Chen, M. Zhu, W. Hu, M. Liu, J. Zhu, H. Ju, *Adv. Funct. Mater.* **2013**, *23*, 2422.

[9] a) H. A. Becerril, J. Mao, Z. Liu, R. M. Stoltenberg, Z. Bao, Y. Chen, *ACS Nano* **2008**, *2*, 463; b) K. Spyrou, M. Calvaresi, E. K. Diamanti, T. Tsoufis, D. Gournis, P. Rudolf, F. Zerbetto, *Adv. Funct. Mater.* **2015**, *25*, 263; c) X.-M. Feng, R.-M., Li, Y.-W. Ma, R.-F. Chen, N.-E. Shi, Q.-L. Fan, W. Huang, *Adv. Funct. Mater.* **2011**, *21*, 2989.

[10] A. Peigney, C. Laurent, E. Flahaut, R. R. Bacsa, A. Rousset, *Carbon* **2001**, *39*, 507.

[11] M. D. Stoller, S. Park, Y. Zhu, J. An, R. S. Ruoff, *Nano Lett.* **2008**, *8*, 3498.

[12] Y. Zhu, S. Murali, W. Cai, X. Li, J. W. Suk, J. R. Potts, R. S. Ruoff, *Adv. Mater.* **2010**, *22*, 3906.

[13] X. Cao, Z. Yin, H. Zhang, *Energy Environ. Sci.* **2014**, *7*, 1850.

[14] Z. Yan, L. Ma, Y. Zhu, I. Lahiri, M. G. Hahm, Z. Liu, S. Yang, C. Xiang, W. Lu, Z. Peng, Z. Sun, C. Kittrell, J. Lou, W. Choi, P. M. Ajayan, J. M. Tour, *ACS Nano* **2013**, *7*, 58.

[15] Z.-D. Huang, B. Zhang, R. Liang, Q.-B. Zheng, S. W. Oh, X.-Y. Lin, N. Yousefi, J.-K. Kim, *Carbon* **2012**, *50*, 4239.

[16] L. Dai, D. W. Chang, J.-B. Baek, W. Lu, *Small* **2012**, *8*, 1130.

[17] P. M. Sudeep, T. N. Narayanan, A. Ganesan, M. M. Shaijumon, H. Yang, S. Ozden, P. K. Patra, M. Pasquali, R. Vajtai, S. Ganguli, A. K. Roy, M. R. Anantharaman, P. M. Ajayan, *ACS Nano* **2013**, *7*, 7034.

[18] J. W. Burress, S. Gadipelli, J. Ford, J. M. Simmons, W. Zhou, T. Yildirim, *Angew. Chem. Int. Ed.* **2010**, *49*, 8902.

[19] A. Nicola, B. G. Sumpter, V. Meunier, *Phys. Chem. Chem. Phys.* **2014**, *16*, 8646.

[20] T. Tsoufis, G. Tuci, S. Caporali, D. Gournis, G. Giambastiani, *Carbon* **2013**, *59*, 100.

[21] F. Guo, W. Xing, J. Zhou, L. Zhao, J. Zeng, Z. Liu, Q. Xue, Z. Yan, *Electrochim. Acta* **2014**, *148*, 220.

[22] W.-S. Hung, C.-H. Tsou, M. De Guzman, Q.-F. An, Y.-L. Liu, Y.-M. Zhang, C.-C. Hu, K.-R. Lee, J.-Y. Lai, *Chem. Mater.* **2014**, *26*, 2983.

[23] S. J. Chae, F. Guenes, K. K. Kim, E. S. Kim, G. H. Han, S. M. Kim, H. Shin, S. Yoon, J. Choi, M. H. Park, C. W. Yang, D. Pribat, Y. H. Lee, *Adv. Mater.* **2009**, *21*, 2328.

[24] K. S. Kim, Y. Zhao, H. Jang, S. Y. Lee, J. M. Kim, K. S. Kim, J. H. Ahn, P. Kim, J. Y. Choi, B. H. Hong, *Nature* **2009**, *457*, 706.

[25] X. S. Li, W. W. Cai, J. H. An, S. Kim, J. Nah, D. X. Yang, R. Piner, A. Velamakanni, I. Jung, E. Tutuc, S. K. Banerjee, L. Colombo, R. S. Ruoff, *Science* **2009**, *324*, 1312.

[26] C. Berger, Z. M. Song, T. B. Li, X. B. Li, A. Y. Ogbazghi, R. Feng, Z. T. Dai, A. N. Marchenkov, E. H. Conrad, P. N. First, W. A. De Heer, *J. Phys. Chem. B* **2004**, *108*, 19912.

[27] J. N. Coleman, *Acc. Chem. Res.* **2013**, 46, 14.

[28] A. A. Green, M. C. Hersam, *J. Phys. Chem. Lett.* **2010**, *1*, 544.

[29] X. Y. Zhang, A. C. Coleman, N. Katsonis, W. R. Browne, B. J. van Wees, B. L. Feringa, *Chem. Commun.* **2010**, *46*, 7539.

[30] A. Ciesielski, P. Samorì, *Chem. Soc. Rev.* **2014**, *43*, 381.

[31] M. Quintana, E. Vazquez, M. Prato, *Acc. Chem. Res.* **2013**, *46*, 138.

[32] J. Malig, N. Jux, D. M. Guldi, *Acc. Chem. Res.* **2013**, *46*, 53.

[33] M. Matsumoto, Y. Saito, C. Park, T. Fukushima, T. Aida, *Nat. Chem.* **2015**, *7*, 730.

[34] S. Pei, H.-M. Cheng, *Carbon* **2012**, *50*, 3210.

[35] a) S. Dubin, S. Gilje, K. Wang, V. C. Tung, K. Cha, A. S. Hall, J. Farrar, R. Varshneya, Y. Yang, R. B. Kaner, *ACS Nano* **2010**, *4*, 3845; b) L. Tang, Y. Wang, Y. Li, H. Feng, J. Lu, J. Li, *Adv. Funct. Mater.* **2009**, *19*, 2782.

[36] a) J. M. Mativetsky, E. Treossi, E. Orgiu, M. Melucci, G. P. Veronese, P. Samorì, V. Palermo, *J. Am. Chem. Soc.* **2010**, *132*, 14130; b) M. Yu, Y. Huang, C. Li, Y. Zeng, W. Wang, Y. Li, P. Fang, X. Lu, Y. Tong, *Adv. Funct. Mater.* **2015**, *25*, 324.

[37] H. R. Thomas, A. J. Marsden, M. Walker, N. R. Wilson, J. P. Rourke, *Angew. Chem. Int. Ed.* **2014**, *53*, 7613.

[38] C. Su, K. P. Loh, *Acc. Chem. Res.* **2013**, *46*, 2275.

[39] D. R. Dreyer, H. P. Jia, C. W. Bielawski, *Angew. Chem., Int. Ed.* **2010**, *49*, 6813.

[40] P. V. Kumar, N. M. Bardhan, S. Tongay, J. Wu, A. M. Belcher, J. C. Grossman, *Nat. Chem.* **2014**, *6*, 151.

[41] X.-G. Li, M.-R. Huang, W. Duan, *Chem. Rev.* **2002**, *102*, 2025.

[42] Y. Xu, H. Bai, G. Lu, C. Li, G. Shi, *J. Am. Chem. Soc.* **2008**, *130*, 5856.

[43] D. C. Marcano, D. V. Kosynkin, J. M. Berlin, A. Sinitskii, Z. Sun, A. Slesarev, L. B. Alemany, W. Lu, J. M. Tour, *ACS Nano* **2010**, *4*, 4806.

[44] S. Chen, J. Zhu, X. Wu, Q. Han, X. Wang, *ACS Nano* **2010**, *4*, 2822.

[45] X. Y. Zhang, Y. Huang, Y. Wang, Y. Ma, Z. Liu, Y. Chen, *Carbon* **2009**, *47*, 334.

[46] a) L. Clima, D. Peptanariu, M. Pinteala, A. Salicb, M. Barboiu, *Chem. Commun.* **2015**, *51*, 17529; b) H. J. Kim, I.-S. Bae, S.-J. Cho, J.-H. Boo, B.-C. Lee, J. Heo, I. Chung, B. Hong, *Nanoscale Res. Lett.* **2012**, *7*, 30.

[47] There might be some contribution of NH^+ from protonated NH for the peak at 401 eV, we could not 100 % rule out this possibility.

[48] G. M. Do Nascimento, P. S. M. Barbosa, V. R. L. Constantino, M. L. A. Temperini, *Colloids and Surfaces A: Physicochem. Eng. Aspects* **2006**, *289*, 39.

[49] G. N. R. Tripathi, R. H. Schuler, *Int. J. Radiat. Appl. lnstrum. Part C Radiat. Phys. Chem.* **1988**, *32*, 251.

[50] S. Stankovich, D. A. Dikin, R. D. Piner, K. A. Kohlhaas, A. Kleinhammes, Y. Jia, Y. Wu, S. T. Nguyen, R. S. Ruoff, *Carbon* **2007**, *45*, 1558.

[51] Z. J. Fan, J. Yan, L. J. Zhi, Q. Zhang, T. Wei, J. Feng, M. L. Zhang, W. Z. Qian, F. Wei, *Adv. Mater.* **2010**, *22*, 3723.

[52] Q. Wu, Y. Xu, Z. Yao, A. Liu, G. Shi, *ACS Nano* **2010**, *4*, 1963.

[53] Y. Zhu, S. Murali, M. D. Stoller, K. J. Ganesh, W. Cai, P. J. Ferreira, A. Pirkle, R. M. Wallace, K. A. Cychosz, M. Thommes, D. Su, E. A. Stach, R. S. Ruoff, *Science* **2011**, *332*, 1537.

[54] Z. Niu, J. Chen, H. H. Hng, J. Ma, X. D. Chen, *Adv. Mater.* **2012**, *24*, 4144.

[55] S. Liu, X. Liu, Z. Li, S. Yang, J. Wang, *New J. Chem.* **2011**, *35*, 369.

[56] S. P. Zhou, H. M. Zhang, Q. Zhao, X. H. Wang, J. Li, F. S. Wang, *Carbon* **2013**, *52*, 440.

[57] P. Si, S. Ding, X.-W. Lou, D.-H. Kim, *RSC Adv.* **2011**, *1*, 1271.

[58] V. Khomenko, E. Frackowiak, F. Béguin, *Electrochim. Acta* **2005**, *50*, 2499.

[59] J. Yan, Q. Wang, T. Wei, Z. Fan, *Adv. Energy Mater.* **2014**, *4*, 1300816.

[60] Due to the presence of the spacers, the conductivity value are lowered, leading to the IR drop in the charge/discharge curves.

[61] The reduction of the surface area of the RG3DCNs is most likely due to aggregation occurring as a result of the lowered dispersibility of the G3DCNs once reduced with hydrazine, followed by a drying up process that increases even further the aggregation.

[62] X. Zhuang, F. Zhang, D. Wu, X. Feng, *Adv. Mater.* **2014**, *26*, 3081.

[63] H. M. Jeong, J. W. Lee, W. H. Shin, Y. J. Choi, H. J. Shin, J. K. Kang, J. W. Choi, *Nano Lett.* **2011**, *11*, 2472.

[64] a) L. Hao, X. Li, L. Zhi, *Adv. Mater.* **2013**, *25*, 3899; b) L.-F. Chen, Z.-H. Huang, H.-W. Liang, H.-L. Gao, S.-H. Yu, *Adv. Funct. Mater.* **2014**, *24*, 5104.

[65] P. J. Hall, M. Mirzaeian, S. I. Fletcher, F. B. Sillars, A. J. R. Rennie, G. O. Shitta-Bey, G. Wilson, A. Cruden, R. Carter, *Energy Environ. Sci.* **2010**, *3*, 1238.

[66] B. G. Choi, J. Hong, W. H. Hong, P. T. Hammond, H. Park, *ACS Nano* **2011**, *5*, 7205.

[67] Z.-S. Wu, Y. Sun, Y.-Z. Tan, S. Yang, X. Feng, K. Müllen, *J. Am. Chem. Soc.* 2012, *134*, 19532.

[68] a) S. W. Lee, N. Yabuuchi, B. M. Gallant, S. Chen, B. S. Kim, P. T. Hammond, Y. Shao-Horn, *Nat. Nanotechnol.* **2010**, *5*, 531; b) J. Liu, J. Jiang, C. Cheng, H. Li, J. Zhang, H. Gong, H. J. Fan, *Adv. Mater.* **2011**, *23*, 2076; c) M. Kim, C. Lee, J. Jang, *Adv. Funct. Mater.* **2014**, *24*, 2489.

[69] S. Park, Y. Hu, J. O. Hwang, E. Lee, L. B. Casabianca, W. Cai, J. R. Potts, H. Ha, S. Chen, J. Oh, S. O. Kim, Y. Kim, Y. Ishii, R. S. Ruoff, *Nat. Commun.* **2012**, *3*, 638.

[70] M. D. Stoller, R. S. Ruoff, *Energy Environ. Sci.* **2010**, *3*, 1294.

[71] Y. Gosotsi, P. Simon, *Science* **2011**, *334*, 917.

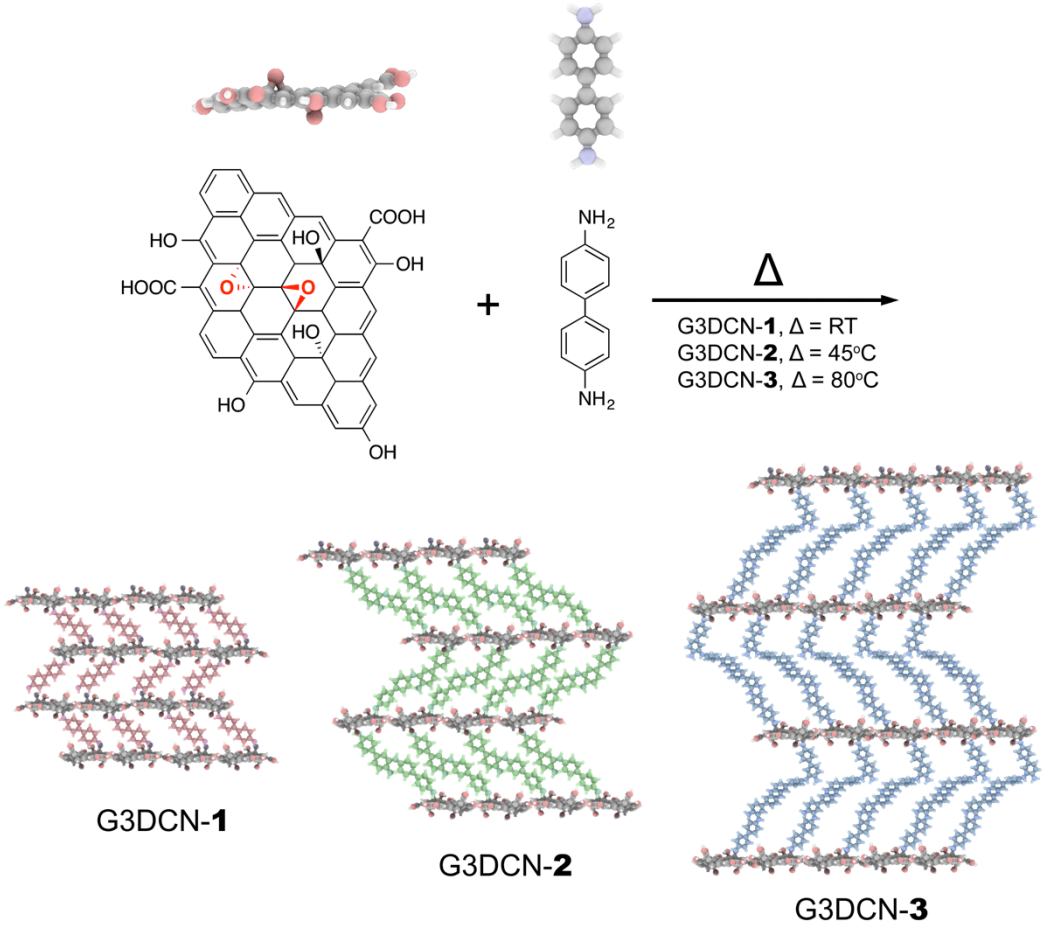

Figure 1. Reaction scheme and simplified representation of G3DCNs. G3DCNs with tunable interlayer distance obtained *via* controlled polymerization of benzidines with graphene oxide at different reaction temperatures. G3DCN-**1** is obtained at room temperature; benzidine units are stitched between GO layers. Upon increase of temperature to 45 or 80 °C, PBZ based polymers, with different degree of polymerization, are covalently connecting GO layers, yielding G3DCN-**2** and G3DCN-**3**, respectively.

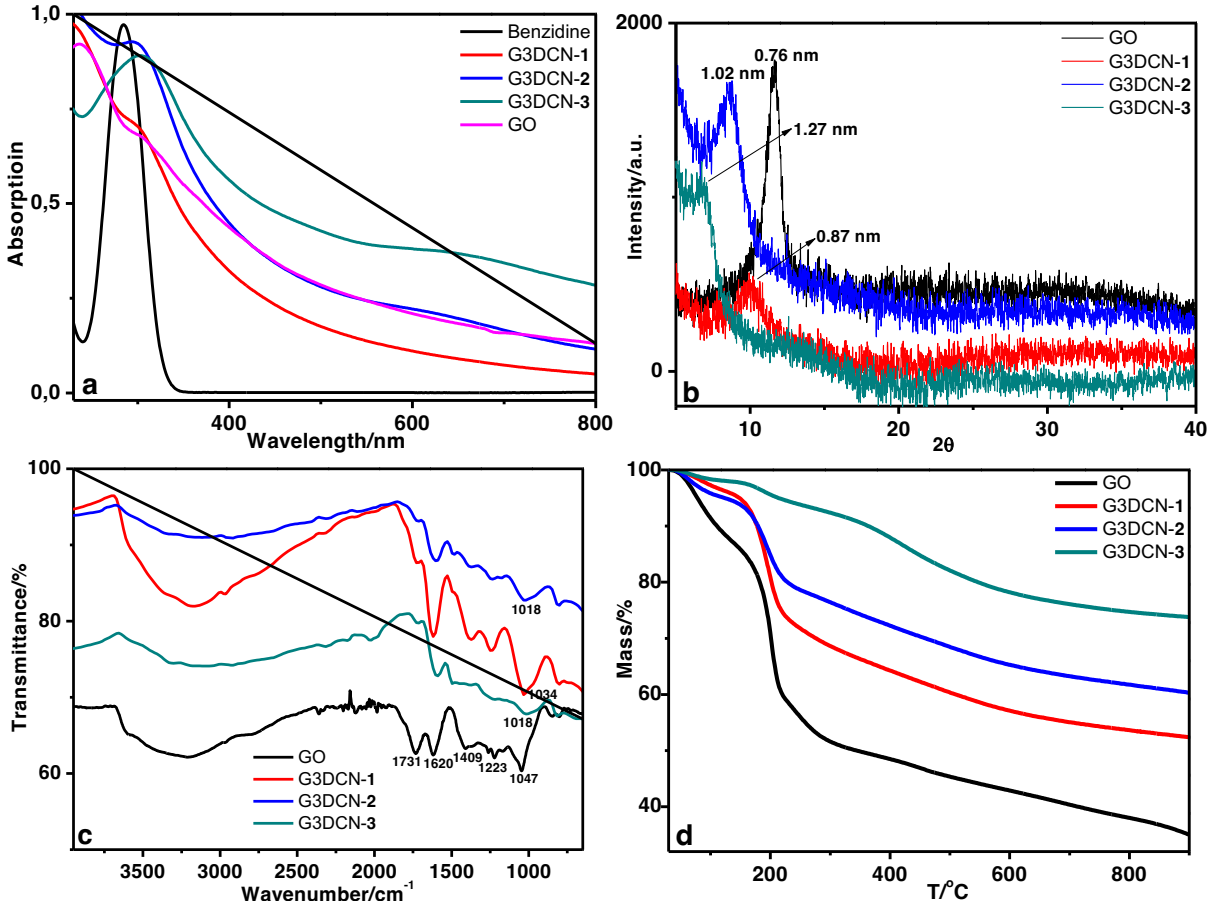

Figure 2. Spectroscopy characterization of GO and the three G3DCNs. (a) UV/Vis absorption spectra recorded in ethanol. G3DCN-**2** and G3DCN-**3** show a broad absorption band within the range of 600 and 700 nm which are ascribed to the characteristic absorption of the oligomers of the PBZ units. (b) Wide-angle X-ray scattering (WAXS) reveals the G3DCN's increased interlayer spacing (from 0.87 up to 1.27 nm) with the reaction temperatures. (c) FTIR spectra evidence the disappearance of epoxy groups and reduction of the carbonyl groups, confirming the successful covalent linkage between GO and the bridges. (d) TGA curves show that the three G3DCNs show an increase of the thermal stability, with G3DCN-**3** being the highest.

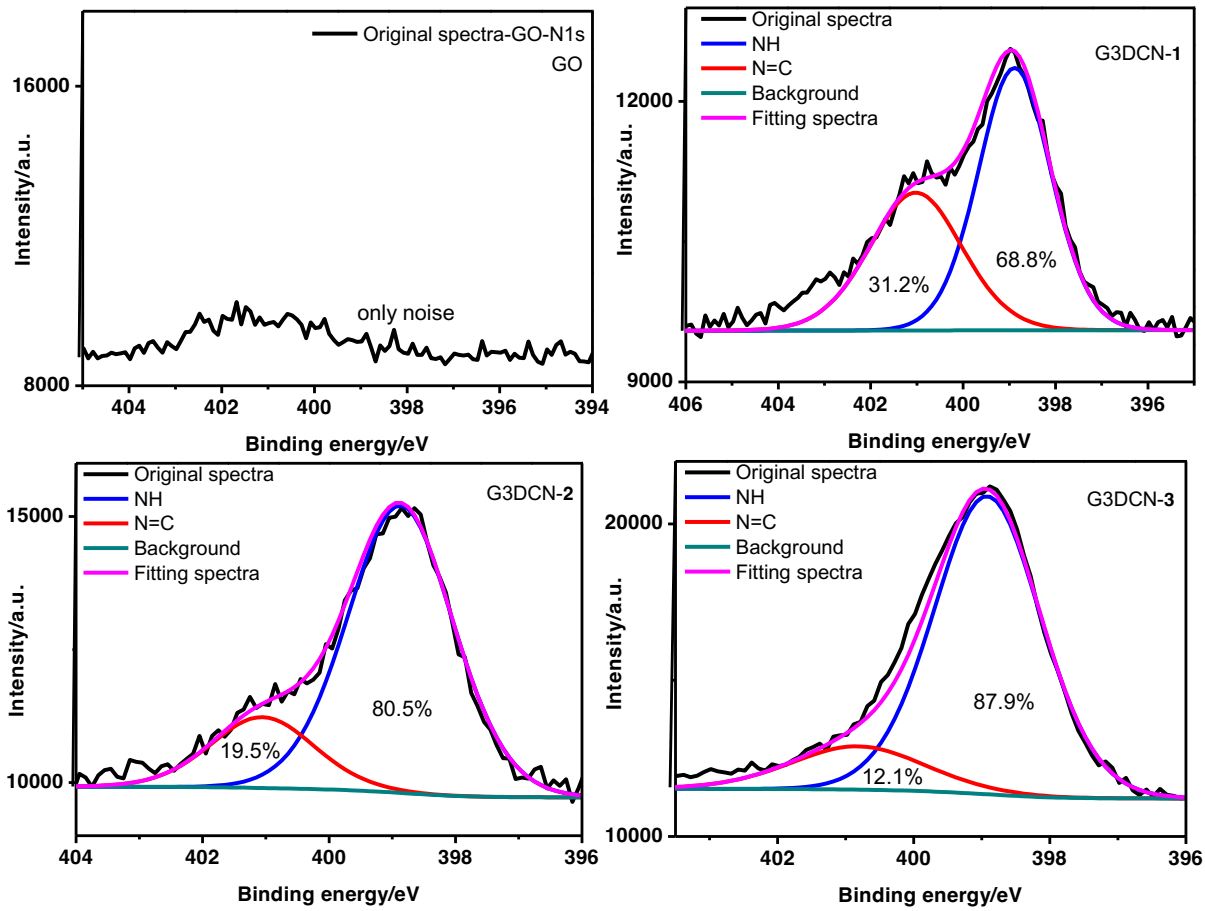

Figure 3. N1s XPS spectra of GO and the three G3DCNs. For all the three G3DCNs samples, the N1s spectra can be deconvoluted in two peaks: the peak at ~ 399 eV is ascribed to –NH, and the peak at around 401 eV is assigned to imine groups. The content of –NH increases with the reaction temperature.

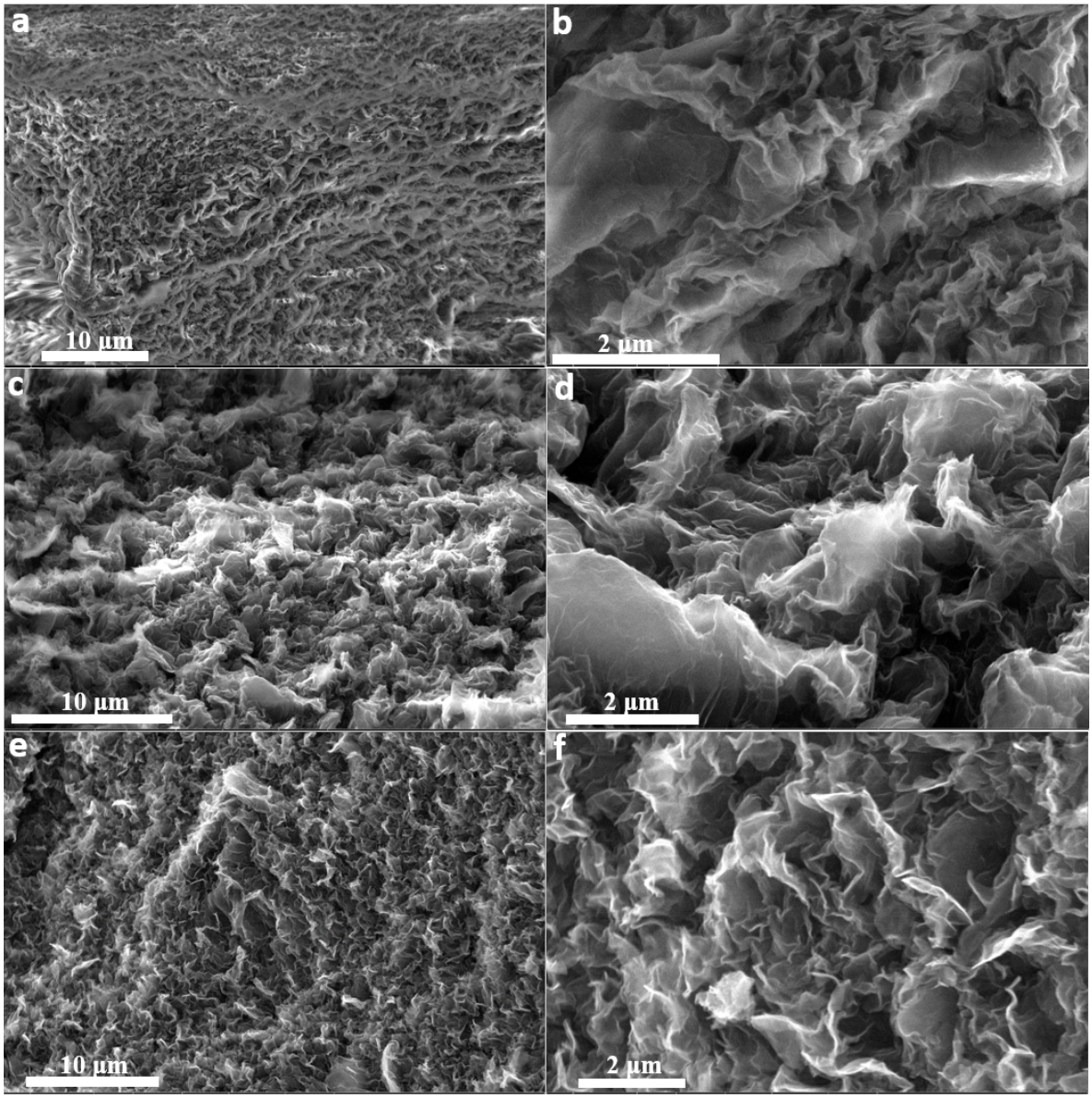

Figure 4. SEM images of the three G3DCNs. (a, b) G3DCN-**1**, (c,d) G3DCN-**2**, and (e,f) G3DCN-**3**. The images show the highly porous structures of the three G3DCNs.

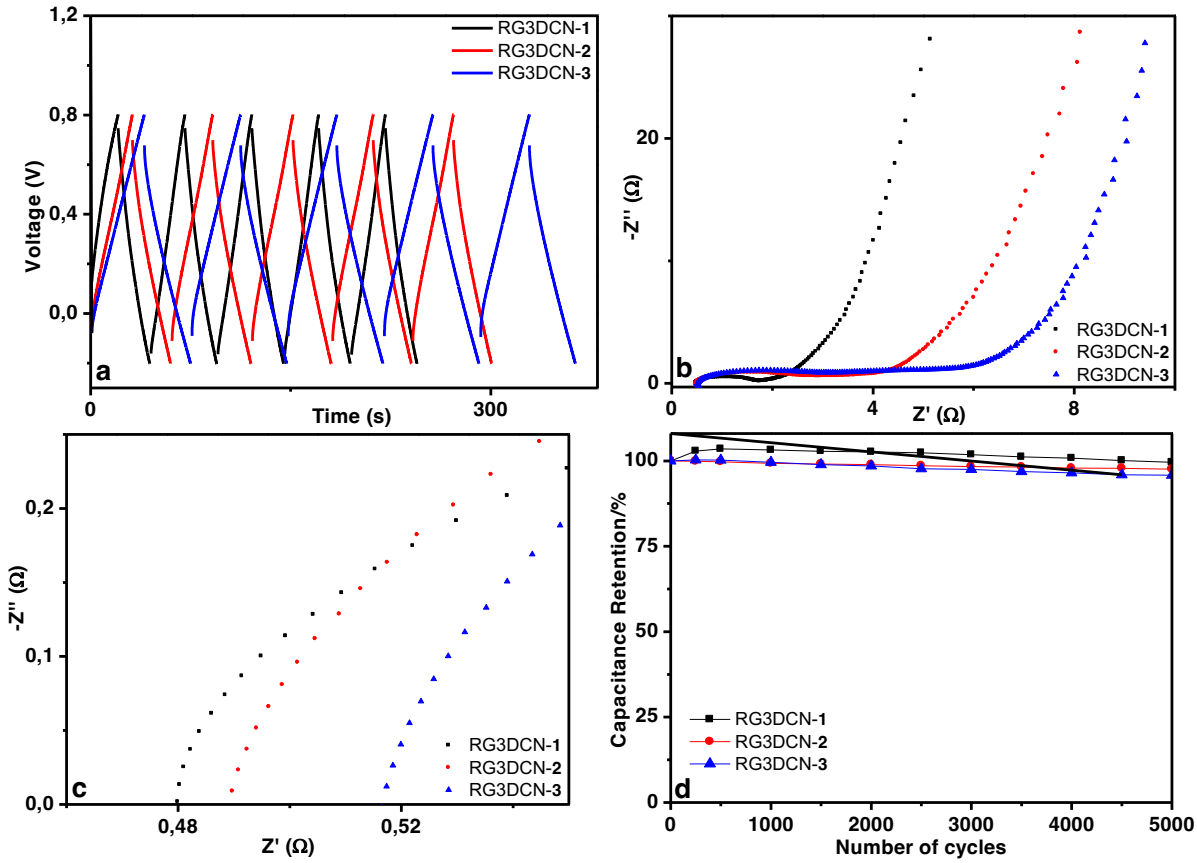

Figure 5. Supercapacitor measurement on the three RG3DCNs in a two-electrode configuration. (a) Galvanostatic charge/discharge curves of the reduced form of G3DCNs: RG3DCN-**1**, RG3DCN-**2** and RG3DCN-**3** at a current density of 1 A g^{-1}. (b) Nyquist plots of RG3DCN-**1**, RG3DCN-**2** and RG3DCN-**3**. (c) An expanded view for the high frequency range of Nyquist plots is shown. (d) Cycle stability of the three RG3DCNs at a current density of 1 A g^{-1}. No obvious specific capacitance loss was observed after 5000 cycles, demonstrating their high stability, long cycle lifetime and good reversibility as electrodes in supercapacitors.